Supporting information

Mesoscale origin of dielectric relaxation with superior electrostrictive strain in bismuth ferrite-based ceramics

Ting Zheng and Jiagang Wu*

Department of Materials Science, Sichuan University, Chengdu, 610064, China

1. Experimental section

$(0.99\text{-}x)Bi_{1.05}Fe_{0.99}Sc_{0.01}O_3\text{-}xBaTiO_3\text{-}0.01Bi_{1.05}(Zn_{0.5}Hf_{0.5})O_3$ (BFS-BT-BZH) ceramics with x=0.3, 0.4, 0.5 have been prepared by conventional solid-state method, details can be seen in our previous report [1]. Temperature/electric field dependent -polarization hysteresis loops (*P*-*E*) and strain curves (*S*-*E*) were measured by ferroelectric measuring equipment (aixACCT TF Analyzer 2000, Germany), at frequency f=2 Hz. The temperature dependence of dielectric constant was tested using LCR analyzer (HP 4980) with frequency 0.5, 1, 10, 100, 300 kHz. Piezoelectric force microscopy (PFM) images were measured using a commercial microscope (MFP-3D, Asylum Research, Goleta, CA) applied to a conductive Pt-Ir coated cantilever EFM-10 (Nano World), with a scanning speed of f=1 Hz and scanning AC voltage of 2 V. In this work, different PFM modes including dual frequency tracking (DART), Vector PFM, and Litho PFM were used to achieve various functional measurements. Raman spectra at room temperature were measured with an excitation source of 532 nm.

2. Results and discussion

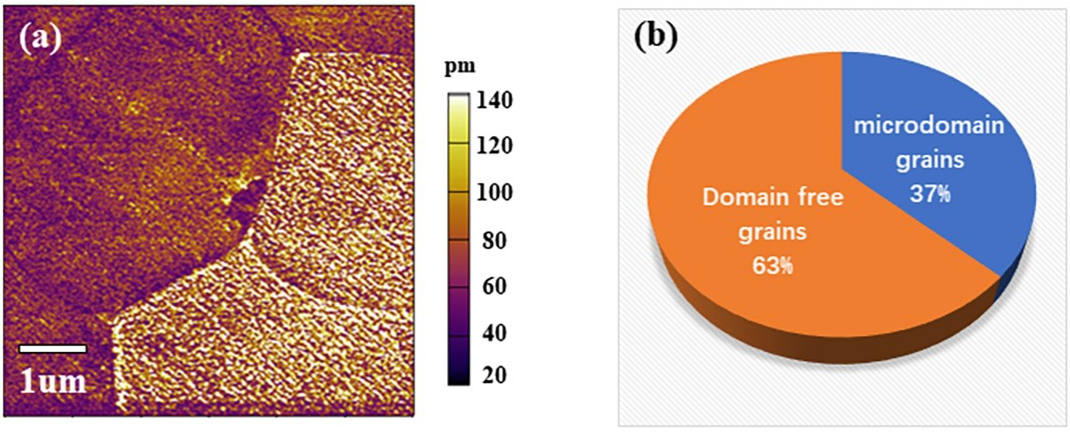

Figure S1: Statistics of two types grains, the total measured grains are 110, distributed at different regions. (a) an example of VPFM amplitude image; (b) statistic map of microdomain grains and domain free grains.

To exclude the accidental phenomenon of the coexistence of two types grains, the statistics of 110 grains (selected randomly at different regions) have been carried out. Fig S1(a) is an example of VPFM amplitude image including both microdomain grains and domain free grains, similar to Fig 2(c). Fig S2(b) shows the statistics of 110 grains, it can be seen that the percentage of microdomain grains is about 37%.

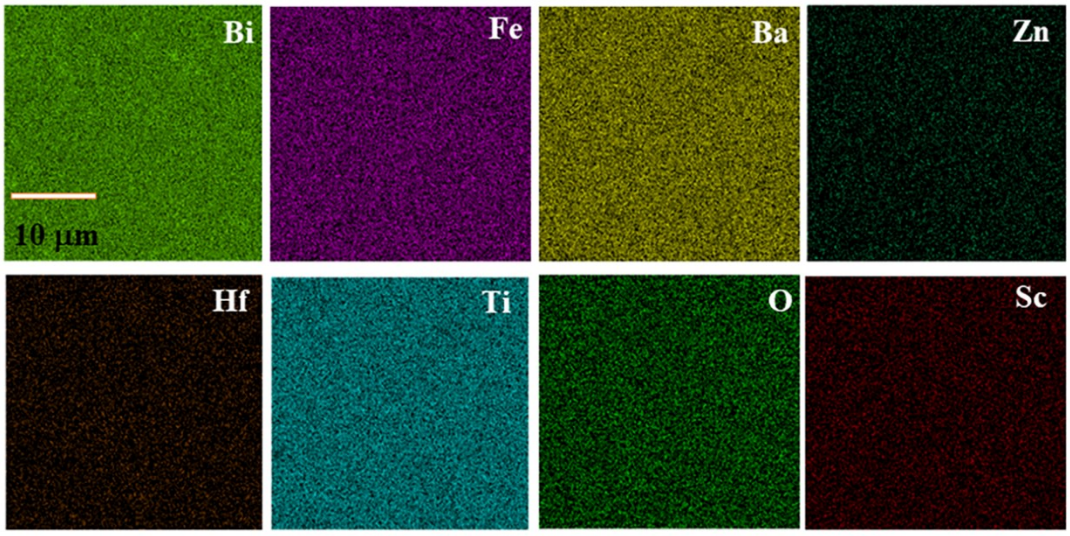

Figure S2: Element mapping of polished surface for x=0.4

Homogenous element distribution can be seen in the x=0.4 sample, although their domain configuration has a strong grain dependence.

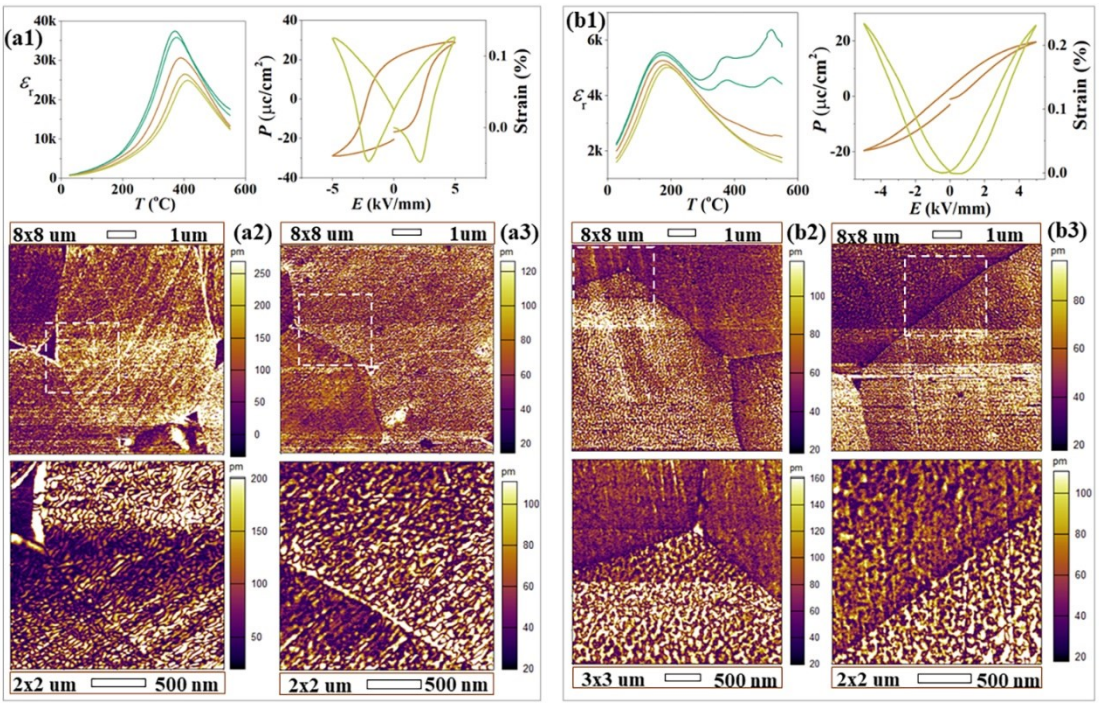

Figure S3: Room temperature electrical properties and domain morphologies of (a1-a3) $Bi_{1.05}FeO_3$-0.3$BaTiO_3$-0.07$Bi(Mg_{2/3}Nb_{1/3})O_3$ (BF-BT-BMN) and (b1-b3) 0.4$BiFeO_3$-0.25$PbTiO_3$-0.35$Pb(Mg_{1/3}Nb_{2/3})O_3$-0.2%MnO_2 (BF-PT-PMN) ceramics: (a1) ε_r-T curves of BF-BT-BMN ceramic, measured at f=0.5 kHz to 300 kHz; P-E and S-E curves measured at f=2 Hz; (a2) VPFM image (8x8 um) and a magnified image (2x2 um, white dashed box in Fig S(a2)) of BF-BT-BMN ceramic; (a3) VPFM images of BF-BT-BMN ceramic, measured at another region. (b1) ε_r-T curves of BF-PT-PMN ceramic, measured at f=0.5 kHz to 300 kHz; P-E and S-E curves measured at f=2 Hz; (a2) VPFM image (8x8 um) and a magnified image (3x3 um, white dashed box in Fig S(b2)) of BF-PT-PMN ceramic; (a3) VPFM images of BF-PT-PMN ceramic, measured at another region.

Fig. S3 shows the electrical properties and domain morphologies of BF-BT-BMN and

BF-PT-PMN ceramics. Obvious dielectric relaxation with different degrees of relaxation can be observed in the two ceramics, leading to the variation of both ferroelectric and strain properties. Similar to that of x=0.4, grain dependence of domain configuration exists in both two samples, indicating that the grain heterogeneity related dielectric relaxation possess universality. In addition, compared with the slim *P-E*/*S-E* loops and grain features with more obvious differences of BF-PT-PMN ceramics, the BF-BT-BMN ceramic has a saturated *P-E* loop and butterfly *S-E* curve due to the grain features with small difference. Therefore, the manipulation of polar nano-structures can be effectively used to regulate electrical properties of BFO-based ceramics.

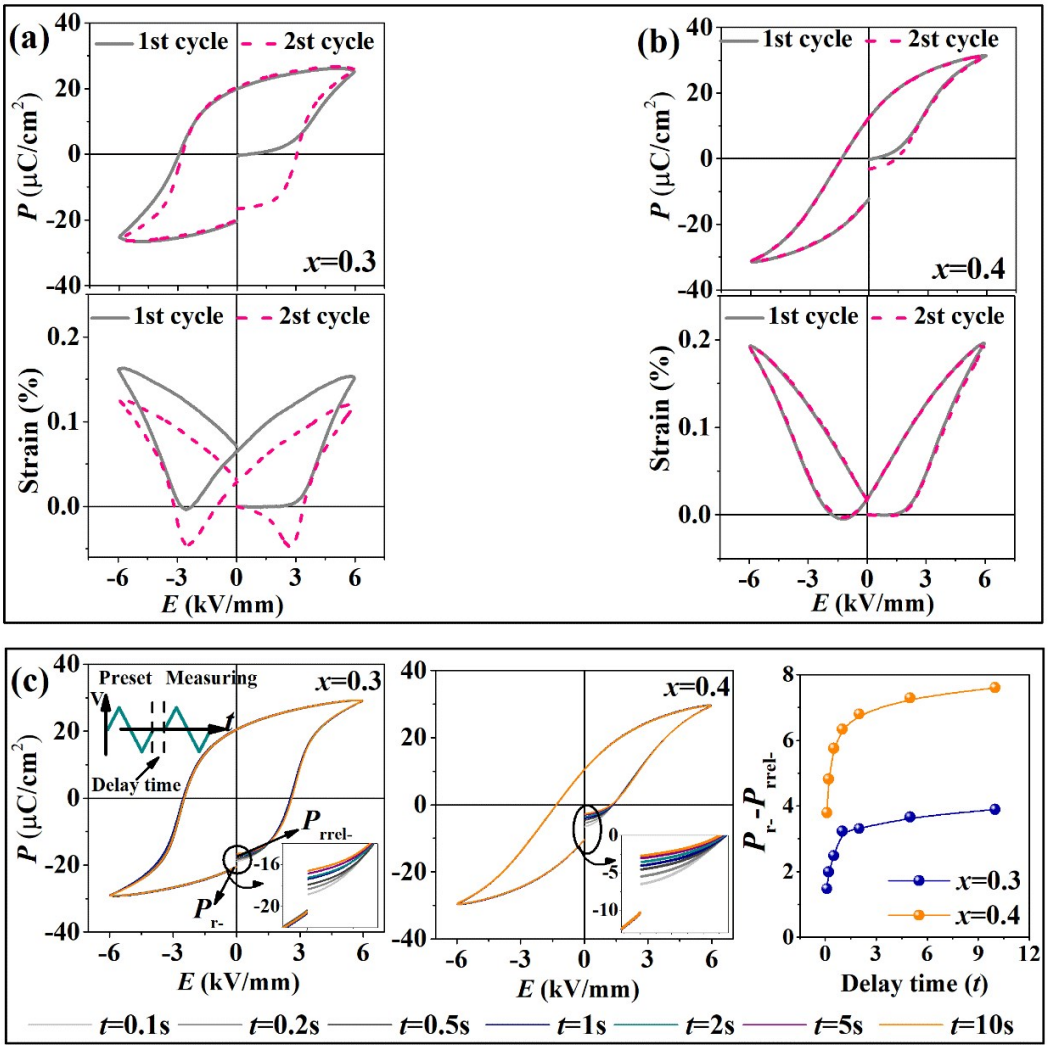

Figure S4: (a-b) first and second cycle *P-E* and *S-E* curves of x=0.3 and x=0.4. (c) *P-E* loops as well as the D-value (P_{r-} -P_{rrel-}) with different delay time of x=0.3 and 0.4.

The first and second cycles of *P-E* loops and *S-E* curves of x=0.3 and 0.4 are displayed in Figs S4(a) and (b). The first cycles are measured from the virgin samples, after which the second cycles are measured. According to previous results, NN and BNT-based ceramics have a large poling strain S1 and a small poling strain S2 due to the electric field induced irreversible phase transition [2, 3]. While in this work, the polarization and strain in first and second cycles almost share the same values regardless of weak relaxor ferroelectric (x=0.3) with obvious non-180 ^{o} domain switching or typical relaxor ferroelectric (x=0.4) without non-180 ^{o} domain switching. In addition, a polarization backswitching with different degree can be also observed in the two samples when the external applied electric field is removed. To confirm the polarization backswitching, *P-E* loops with different delay times are shown in Fig S4(b). Pulse voltage loading mode can be seen in the inset of Fig S4(b). A pre-polarization was induced by a preset pulse, the *P-E* loops shown in Fig S4(c) is obtained by the measuring pulse. The delay time between preset pulse and measuring pulse can be designed to confirm the polarization backswitching degree [4]. If the polarization backswitching happens, the measured initial polarization (P_{rrel-}) will be reduced as compared with the saturated remanent polarization (P_{r-}), because part of preset domains will switch back automatically during the delay time. The difference between P_{r-} and P_{rrel-} is a sign of polarization backswitching, which has been summarized in Fig. S4(c). It is clearly that

the initial polarization (P_{rrel-}) has a strong dependence on delay time. Longer the delay time, greater the backswitching. But on the whole, the backswitching behavior of relaxor ferroelectric (x=0.4) is more serious than that of x=0.3, which is closely related to the domain refinement and activated domain dynamics in relaxor ferroelectrics.

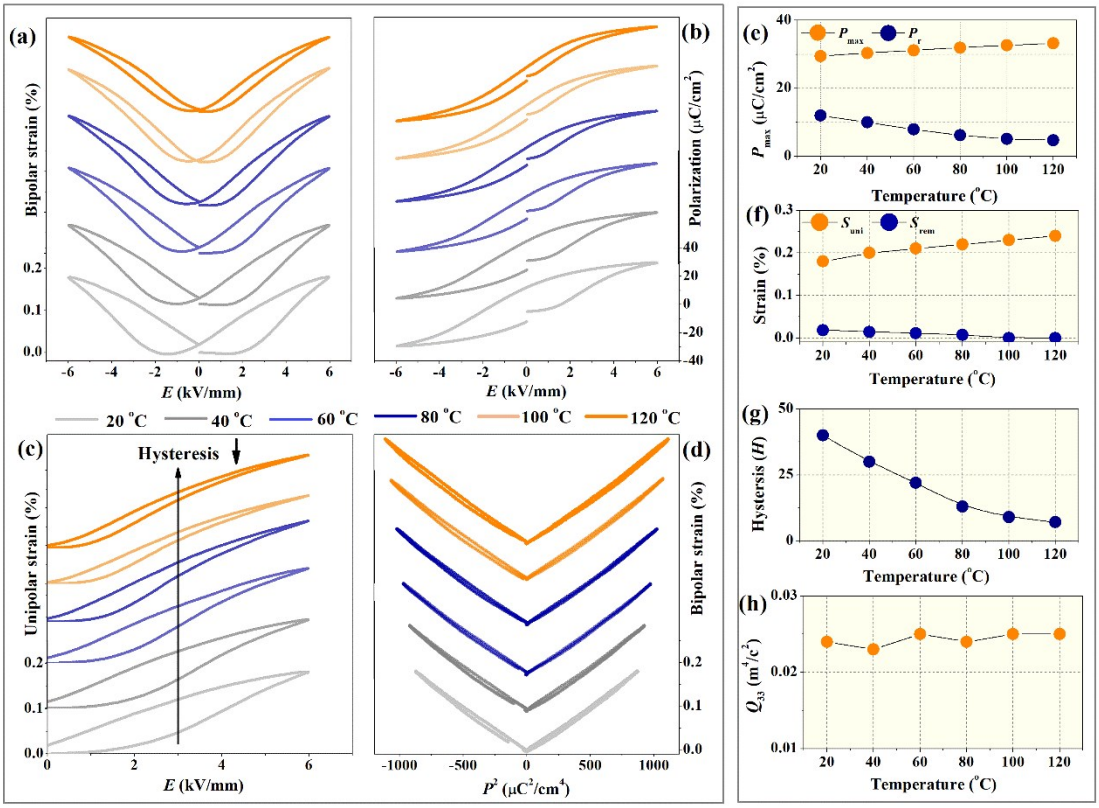

Figure S5: (a) Bipolar *S*-*E* curves, (b) *P*-*E* loops, (c) unipolar *S*-*E* curves, (d) *S*-P^2 curves of x=0.4 as a function of temperature, measured at f=2 Hz and E=6 kV/mm. (e-h) Temperature dependence of (e) polarization, (f) strain, (g) hysteresis, and (h) Q_{33} values, all data derived from Fig S5(a-d).

Fig S5 (a-d) shows the temperature dependence of bipolar *S*-*E*, *P*-*E*, unipolar *S*-*E*, and *S*-P^2 curves of x=0.4, measured under 20~120 °C and 6 kV/mm. The unipolar strain (S_{uni}) and maximum polarization (P_{max}) gradually increase with increasing temperature.

While the remanent strain (S_{rem}) and remanent polarization (P_r) gradually decrease with increasing temperature, leading to the decreased hysteresis in both *S-E* curves and *P-E* loops. The evolution of strain and ferroelectric properties with temperature is correlative to the changing trend of *in-situ* temperature-dependent d_{33} [Fig 1], which is closely related to the concentration transformation between strong piezo-response and weak piezo-response grains. According to the evolution of *P-E* and *S-E* loops, all the S-P^2 curves under different temperatures follow theoretically derived quadratic relation with nearly linear and hysteresis free behavior, and the derived Q_{33} values are almost independent to temperature [Fig S5(h)].

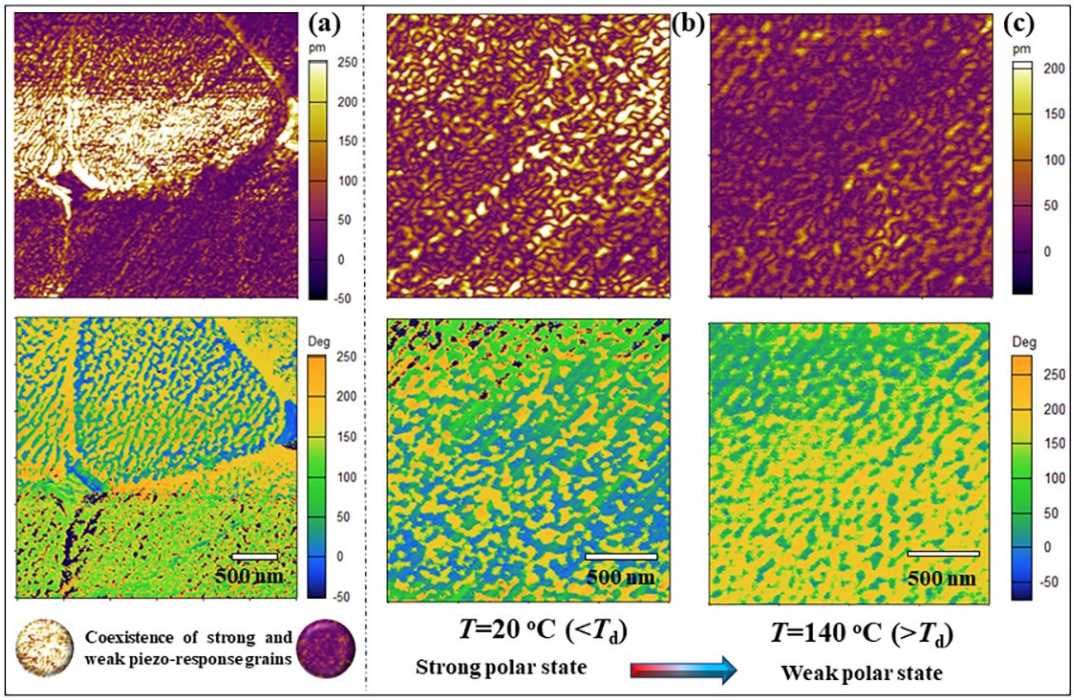

Figure S6: (a) VPFM amplitude and phase images with both strong piezo-response grains and weak piezo-response grains, measured at room temperature. VPFM amplitude and phase images of the strong piezo-response grain measured at (b) T=20 °C ($<T_d$) and (c) T=140 °C ($>T_d$), showing the transition from strong polar state to weak

polar state controlled by T_d.

Fig S6(a) shows the VPFM amplitude and phase images of x=0.4, reflecting the coexistence of both strong piezo-response grains and weak piezo-response grains again. To reveal the property evolution under thermal excitation, temperature dependence of domain configuration of strong piezo-response grain has been presented in Fig S6(b-c), measured at T=20 ^{o}C ($<T_d$) and 140 ^{o}C ($>T_d$). Different from the stable domain configuration under different temperatures in ferroelectrics (x=0.265) [1], obvious temperature-dependent nanodomain influenced by depolarization temperature (T_d) can be observed in relaxor ferroelectrics (x=0.4). For example, weaker piezo-response and chaotic domain contrast appear when T=140 ^{o}C, suggesting that the strong piezo-response polar cluster state ($<T_d$) will transform into weak piezo-response polar entities state ($>T_d$). As a result, the property evolution (piezoelectricity and ferroelectricity) caused by T_d can be well interpreted by the evolution of domain configurations.

References:

[1] T. Zheng, J. G. Wu. Perovskite $BiFeO_3$-$BaTiO_3$ ferroelectrics: engineering property by domain evolution and thermal depolarization modification. Adv. Electron. Mater., 2020, 6, 2000079.

[2] J. Yin, G. Liu, X. Lv, Y. X. Zhang, C. L. Zhao, B. Wu, X. M. Zhang, J. G. Wu. Superior and anti-fatigue electro-strain in $Bi_{0.5}Na_{0.5}TiO_3$-based polycrystalline relaxor ferroelectrics. J. Mater. Chem. A., 2019, 7, 5391

[3] M. X. Dou, J. Fu, R. Z. Zuo. Electric field induced phase transition and accompanying giant poling strain in lead-free $NaNbO_3$-$BaZrO_3$ ceramics. J. Eur.

Ceram. Soc. 2018, 38, 3104-3110.

[4] Y. Zhou, C. Wang, X. J. Lou, S. L. Tian, X. K. Yao, C. Ge, E. J. Guo, M. He, G. Z. Yang, K. J. Jin. Internal electric field and polarization backswitching induced by Nb doping in $BiFeO_3$ thin films. ACS Appl. Electron. Mater., 2019, 1, 2701-2707.